Loss of the Forkhead Transcription Factor FoxM1 Causes Centrosome Amplification and Mitotic Catastrophe

Diane R. Wonsey and Maximillian T. Follettie

Department of Discovery Medicine, Wyeth Research, Cambridge, Massachusetts

Abstract

Expression of the forkhead transcription factor FoxM1 correlates with proliferative status in a variety of normal and transformed cell types. Elevated expression of FoxM1 has been noted in both hepatocellular carcinoma and basal cell carcinoma. However, whether FoxM1 expression is essential for the viability of transformed cells is unknown. We report here that the expression of FoxM1 is significantly elevated in primary breast cancer. Microarray analysis shows that FoxM1 regulates genes that are essential for faithful chromosome segregation and mitosis, including *Nek2, KIF20A*, and *CENP-A*. Loss of FoxM1 expression generates mitotic spindle defects, delays cells in mitosis, and induces mitotic catastrophe. Time-lapse microscopy indicates that depletion of FoxM1 generates cells that enter mitosis but are unable to complete cell division, resulting in either mitotic catastrophe or endoreduplication. These findings indicate that FoxM1 depletion causes cell death due to mitotic catastrophe and that inhibiting FoxM1 represents a therapeutic strategy to target breast cancer. (Cancer Res 2005; 65(12): 5181-9)

Introduction

The forkhead box (FOX) protein family consists of ~50 proteins that are characterized by a conserved 100 amino acid winged-helix DNA binding domain. FoxM1 was originally identified in a screen designed to clone cDNAs encoding proteins recognized by the MPM2 antibody, which recognizes an amino acid epitope found on M phase phosphoproteins (1). A partial cDNA sequence corresponding to *FoxM1* was identified, indicating that FoxM1 is phosphorylated in mitosis and is involved in the G_2-M phase of the cell cycle. Detailed cell cycle analysis revealed that expression of the FoxM1 protein increases during G_1 and S phase, reaching maximal levels in G_2-M (2). Evidence suggesting that FoxM1 is required for coupling DNA replication with mitosis is provided by the observation that hepatocytes and cardiomyocytes from *FoxM1*$^{-/-}$ mice are polyploid. Mice lacking *FoxM1* die in the perinatal period, with noticeable defects in the myocardium, including irregular cellular orientation and enlarged nuclei with up to a 50-fold increase in DNA content (3). Although FoxM1 is widely expressed in embryonic tissues (4), the defects in *FoxM1*$^{-/-}$ mice are restricted to tissues that normally become polyploid in adult mice. Terminally differentiated, nonproliferating tissues display relatively low levels of FoxM1 expression (5). Several studies indicate that FoxM1 participates in cell cycle control. Mice with a targeted deletion of FoxM1 in the liver show decreased bromodeoxyuridine (BrdUrd) incorporation and fewer mitotic cells compared with wild-type controls following partial hepatectomy (6). Conversely, premature expression of FoxM1 in transgenic mice accelerates hepatocyte DNA replication and the expression of cell cycle regulatory proteins following partial hepatectomy (7).

Consistent with a role in proliferation, elevated expression of *FoxM1* has been reported in both basal cell carcinoma (8) and in hepatocellular carcinoma (9). In addition, FoxM1 expression is required for the proliferative expansion of hepatocellular carcinoma in a mouse model of tumor induction (10). The observation that a $p19^{ARF}$ peptide fragment physically interacts with FoxM1, suppresses FoxM1 transcriptional activity, and inhibits FoxM1-enhanced anchorage-independent growth (10) suggests that FoxM1 may be an attractive target for cancer therapy. However, it has not been determined whether FoxM1 is essential for viability in established cancer cells or whether specifically inhibiting FoxM1 is an effective therapeutic strategy.

Centrosomes are the primary components of the microtubule organizing center in mammalian cells. Immediately after mitosis, each daughter cell contains a single centrosome. In most cell types, centrosome duplication begins in S phase, and the two daughter centrosomes form the poles of the mitotic spindle. The regulation of centrosome duplication in mammalian cells is tightly controlled in order to maintain genomic integrity and prevent aneuploidy (11). In addition to directing the formation of the mitotic spindle, recent evidence indicates that the centrosome participates in cell cycle regulation (12, 13), and this activity is independent of microtubule nucleating activity. Cancer cells frequently contain elevated numbers of centrosomes (14, 15), although whether centrosome amplification contributes to transformation or is a consequence of cancer progression remains to be determined. Because centrosomes usually nucleate microtubules, cells with supernumerary centrosomes form multipolar mitotic spindles and may undergo mitotic catastrophe (16).

Mitotic catastrophe is defined as a form of cell death that occurs during mitosis, often arising from aberrant G_2 checkpoint control (17). In normal cells, the G_2 checkpoint is activated by DNA damage and involves a complex network of genes involved in cell cycle arrest, DNA repair, and apoptosis (18). Failure of the G_2 checkpoint allows premature progression through mitosis, resulting in mitotic catastrophe. Although the molecular details of mitotic catastrophe remain to be defined, several genes involved in the G_2 checkpoint induce mitotic catastrophe when disrupted, including *14-3-3σ* (19), *ATR* (20), and the *CHK1* kinase (21). In addition, defects in proteins required for mitotic spindle assembly also induce catastrophe. Depletion of hNuf2, a kinetochore protein involved in microtubule attachment, arrests cells in prometaphase and induces mitotic cell death (22). Because mitotic catastrophe, by definition, is only induced in proliferating cells, and also occurs following DNA damage in cells with mutations in checkpoint proteins, induction of catastrophe

Note: Supplementary data for this article are available at Cancer Research Online (http://cancerres.aacrjournals.org/).

Requests for reprints: Diane R. Wonsey, Dana Farber Cancer Institute, 44 Binney Street, Mayer 649, Boston, MA 02115. Phone: 617-582-7944; E-mail: Diane_Wonsey@dfci.harvard.edu.

presents a promising opportunity for specifically targeting cancer cells.

Analysis of microarray data from primary breast cancers revealed that *FoxM1* expression is increased in infiltrating ductal carcinoma, the most commonly diagnosed form of breast cancer. In order to evaluate whether FoxM1 expression is essential for cancer cell growth or is secondary to an increase in the number of proliferating cells, we used short interfering RNA (siRNA) to evaluate the effect of directly inhibiting FoxM1 in breast cancer cell lines. Microarray data from cells treated with FoxM1 siRNA identified several previously unreported genes that are regulated by FoxM1, including *CENP-A, Nek2*, and *KIF20A*. Using a stable FoxM1 hairpin construct, we found that continuous depletion of FoxM1 results in mitotic catastrophe. Our results indicate that FoxM1 is required for cancer cell viability and show that loss of FoxM1 causes aberrant spindle formation, ultimately leading to mitotic catastrophe.

Materials and Methods

Primary tissue expression profiling data. Expression profiling data from primary human cancer samples was obtained from the GeneLogic BioExpress Database (Gaithersburg, MD), a commercially available repository of transcriptional profiling data from thousands of diseased and normal tissue samples. Whole tumor samples from patients with infiltrating ductal carcinoma (n = 194) were chosen at random from the database. Normal samples (n = 14) were taken from patients undergoing reduction mammoplasty. Data from patients with fibrocystic breast disease (n = 10) and fibroadenoma (n = 7) were filtered to remove patients with concomitant malignant disease elsewhere in the breast at the time of surgery. RNA from each sample was analyzed on Affymetrix HgU95A chips and normalized with MAS 4.0. Difference averages for qualifier 34715_at were used for statistical analysis, and negative difference averages were assigned a value of 1. P values were calculated using the Mann-Whitney U test.

TaqMan analysis. Breast cancer and adjacent normal tissue samples, with accompanying clinical data, were obtained from Genomics Collaborative (Cambridge, MA). Tumor samples were from patients with stage II and stage III infiltrating ductal carcinomas, and contained 65% to 75% tumor tissue. Real-time reverse transcription-PCR was done using the forward primer 5′-GACAGGTTAAGGTTGAGGAGCCT-3′, reverse primer 5′-GTGCTGTTGATGGCGAATTGT-3′, and FAM-labeled probe 5′-TGTCTGAGCGGCCACCCTACTCTTACA-3′. TaqMan one-step RT-PCR Master Mix Reagents (Applied Biosystems, Foster City, CA) were used for reverse transcription and real-time PCR according to the manufacturer's instructions. The predeveloped assay reagent Human ribosomal protein PO (Applied Biosystems) was used as a control for normalizing FoxM1 expression. Relative amounts of transcript were determined by generating a standard curve with human Universal Reference RNA (BD Clontech, Palo Alto, CA). Reactions were done in triplicate and the average and SD are shown. Fold change represents the ratio of FoxM1 in cancer tissue as compared with the adjacent normal tissue.

Cell culture. All cell lines were obtained from American Type Culture Collection (Manassas, VA). MCF-7, BT-474, SK-BR-3, and MDA-468 cells were cultured in DMEM with 10% fetal bovine serum. BT-20 cells were maintained in Eagle's minimum essential medium with 10% fetal bovine serum. MCF-12A cells were cultured in a 1:1 mixture of DMEM and Ham's F12 medium, 20 ng/mL human epidermal growth factor, 100 ng/mL cholera toxin, 0.01 mg/mL bovine insulin, 500 ng/mL hydrocortisone, and 5% horse serum. MCF-10A cells were grown in MEGM made of MEBM basal medium and SingleQuot additives (Clonetics, CC-3150), supplemented with 100 ng/mL cholera toxin.

RNAi. Annealed, purified, double-stranded oligonucleotides were obtained from Dharmacon (Lafayette, CO). The FoxM1 siRNA sequence was CCUUUCCCUGCACGACAUGdTdT. The green fluorescent protein (GFP) control oligo sequence was CAAGCUGACCCUGAAGUUCdTdT. For transfections, cells were plated at ~50% confluence and transfected with 200 nmol/L oligo using siPORT (Ambion, Austin, TX) for 5 hours according to the manufacturer's instructions. Stable expression of the FoxM1 short hairpin RNA (shRNA) was achieved using the pSilencer 3.1 H1 puro vector (Ambion), with a FoxM1 hairpin sequence based on the FoxM1 siRNA indicated above, according to the manufacturer's instructions for hairpin design. The negative control vector is pSilencer 3.1 H1 puro, containing a 66-bp hairpin with limited homology to known sequences in the human genome, supplied by the manufacturer (Ambion). Cells were transfected with Effectene transfection reagent (Qiagen, Valencia, CA) and selected for 6 days in the presence of 0.5 μg/mL puromycin.

Cell proliferation assays. The cell proliferation reagent WST-1 (Roche, Indianapolis, IN) was used to assay cell number. Cells were trypsinized 24 hours after transfection and plated in 96-well plates. Absorbance was assayed 30 minutes after adding WST-1 according to the manufacturer's instructions.

Immunoblot analysis. Culture cells were lysed in buffer containing 10 mmol/L Tris (pH 7.4), 1% SDS, 1 mmol/L sodium orthovanadate, and complete protease inhibitors (Roche). Protein concentrations were analyzed using the bicinchoninic acid assay (Pierce, Rockford, IL), and equivalent amounts of protein were loaded on 12% SDS-PAGE gels. Proteins were transferred to Optitran nitrocellulose (Schleicher & Schuell, Keene, NH) and blotted with antibodies against FoxM1 (MPP2 K-19, Santa Cruz, Santa Cruz, CA) or β-actin (A-5441, Sigma, St. Louis, MO).

Microarray analysis. BT-20 cells were transfected in triplicate with a mock transfection (no siRNA), GFP siRNA, or FoxM1 siRNA. Cells were collected 48 hours after transfection, and RNA was isolated using the RNeasy Mini Kit (Qiagen). Generation of labeled target for hybridization was essentially as described (23). Briefly, 8 μg of total RNA was used to generate first-strand cDNA using a T7-oligo d(T) primer. Following second-strand synthesis, *in vitro* transcription was done using biotinylated CTP and UTP (Enzo Diagnostics, Farmingdale, NY). Fifteen micrograms of biotinylated RNA was fragmented prior to overnight hybridization on Affymetrix HgU133A arrays. Arrays were analyzed and absent/present calls were determined with Affymetrix GeneChip software. Transcript abundance was calculated by comparing the signal value of each transcript to the signal value of a cRNA spike-in standard curve (24). Fold change analysis was done using the average of mock and GFP-transfected cells (n = 6 in total) relative to the average of FoxM1 siRNA-transfected cells (n = 3). P values were calculated using Student's t test. Data were filtered using a fold change cutoff of $\pm$1.70, a P value $\leq$ 0.010000, and at least 3 of 9 "present" calls for each probe set. The entire data set has been deposited in the National Center for Biotechnology Information's Gene Expression Omnibus (GEO, http://www.ncbi.nlm.nih.gov/geo/) and is accessible through GEO Series accession number GSE2222.

Crystal violet staining. Following transfection, 2.5×10^5 cells per well were plated in six-well dishes. At the indicated times, cells were fixed in 0.5% glutaraldehyde, washed, and stained with 0.2% crystal violet.

Time-lapse imaging. Cells in six-well dishes were placed in CO_2-independent medium (Life Technologies, Carlsbad, CA), overlaid with mineral oil, and maintained at 37°C. Phase contrast images were captured at regular intervals using an Olympus IMT-2 inverted microscope equipped with a Zeiss AxioCam HRC digital imaging system.

BrdU assay. Cells were labeled for 20 hours with BrdU and analyzed with the BrdU Labeling and Detection Kit (Roche Applied Science) according to the manufacturer's instructions. Cells were examined by fluorescence microscopy and scored for BrdU staining. The percentage of BrdU-positive cells was obtained from at least 200 nuclei for each sample.

Immunohistochemistry. Cells were plated on glass coverslips coated with poly-D-lysine and allowed to adhere overnight. For analysis of α tubulin, cells were fixed in 3% paraformaldehyde/PBS for 20 minutes, washed in PBS, and permeabilized with 0.5% Triton X-100 for 3 minutes. Blocking was done with 5% bovine serum albumin in PBS for 6 hours. Monoclonal α-tubulin antibody (Sigma clone B-5-1-2) was diluted 1:1,000 in 3% bovine serum albumin/PBS, incubated overnight at 4°C, and detected with AlexaFluor 488 goat anti-mouse IgG (Molecular Probes, Eugene, OR). For detection of centrosomes, cells were fixed with a 1:1 mixture of

acetone/methanol at −20°C for 10 minutes and incubated with γ-tubulin monoclonal antibody (clone GTU-88) from Sigma at a dilution of 1:2,000. All other steps were identical to the staining for α-tubulin. Cells were counterstained with 4′,6-diamidino-2-phenylindole before mounting with ProLong antifade reagent (Molecular Probes). The percentage of cells with mitotic spindle defects was determined by counting 100 mitotic cells from three different transfections for both negative control and FoxM1 shRNA. Cells were scored as abnormal if they displayed spindles with more than two poles. The percentage of cells with more than two centrosomes was determined by counting at least 200 cells from three different transfections for negative control and FoxM1 shRNA.

Results

The *FoxM1* transcript is significantly increased in primary infiltrating ductal carcinomas. In order to identify transcripts that are specifically increased in breast cancer, we have analyzed Affymetrix HgU95A data from 194 infiltrating ductal carcinomas present in the GeneLogic BioExpress database, a commercially available collection of transcriptional profiling data. Comparison of ductal carcinoma and normal breast tissue identified a transcript, *FoxM1*, which was increased relative to normal tissue (Fig. 1*A*). The *FoxM1* transcript was significantly elevated in breast cancer relative to normal breast tissue (Mann-Whitney *U* test *P* value = 1.6×10^{-8}), fibrocystic breast disease ($P = 6.0 \times 10^{-8}$), and fibroadenomas ($P = 0.0012$), indicating that *FoxM1* expression is specifically elevated in infiltrating ductal carcinomas. In order to confirm the microarray data, real-time reverse transcription-PCR analysis was done on matched tissue samples from stage II and III ductal carcinomas and adjacent normal tissue (Fig. 1*B*). The two stage II carcinomas showed an increase of 4- or 9-fold relative to adjacent normal tissue, whereas the stage III carcinomas showed an increase of 76- or 116-fold. We then examined whether FoxM1 was also overexpressed in breast cancer cell lines, using two nontransformed, spontaneously immortalized breast epithelial cell lines, MCF-10A and MCF-12A, for comparison. Western blotting of five transformed breast cancer cell lines shows that the FoxM1 protein is increased in all five lines relative to the two nontransformed lines (Fig. 1*C*). Both of the nontransformed cell lines proliferate more rapidly than either BT-20 or MCF-7 breast cancer cells (Supplemental Fig. S1), suggesting that elevated expression of FoxM1 is specific to transformed cells, rather than representing a secondary consequence of heightened proliferation. These results confirm that *FoxM1* expression is increased in primary infiltrating ductal carcinoma and that the FoxM1 protein is consistently overexpressed in breast cancer cell lines.

FoxM1 short interfering RNA inhibits proliferation in BT-20 and MCF-7 breast cancer cell lines. In order to address whether FoxM1 is essential for the proliferation of breast cancer epithelial cells, we did RNAi using transient transfection of a 21-nucleotide double-stranded RNA molecule that recognizes all three splice forms of *FoxM1* (25). MCF-7 estrogen receptor–positive and BT-20 estrogen receptor–negative cell lines were transfected with FoxM1 siRNA, and cells were collected for protein analysis at the indicated time points (Fig. 2*A* and *B*). Immunoblotting indicates that FoxM1 siRNA reduces expression of the FoxM1 protein, whereas FoxM1 expression in mock-transfected and GFP-transfected cells remains unchanged. Although both cells lines were transfected under similar conditions, the decrease in FoxM1 protein expression was less pronounced and returned within 72 hours in MCF-7 cells, whereas expression did not return until 120 hours in the BT-20 cell line. Differences in transfection efficiency may account for this observation.

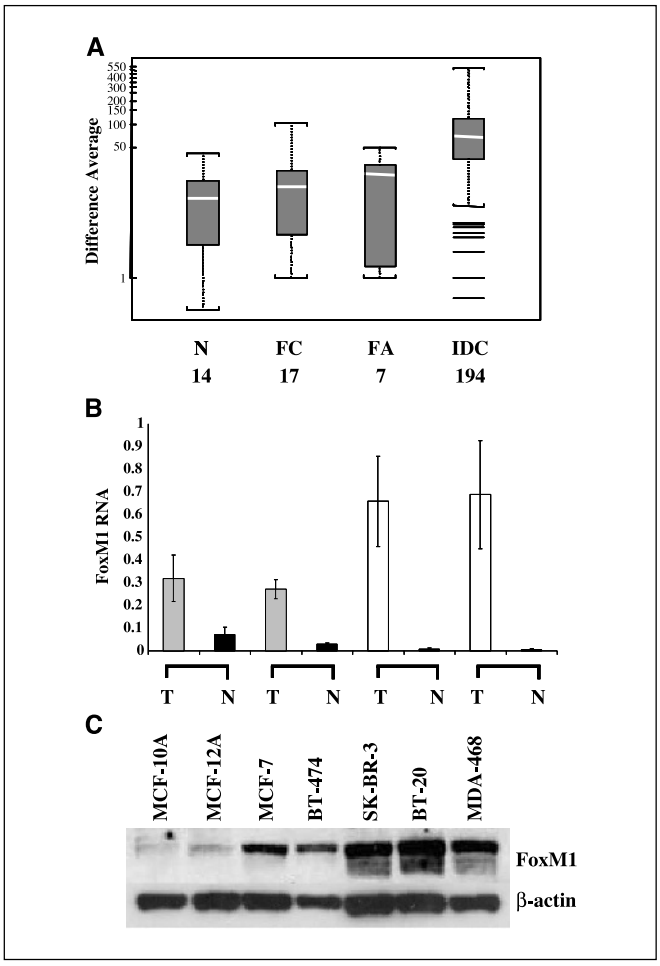

Figure 1. FoxM1 is overexpressed in human breast cancer and breast cancer cell lines. *A, FoxM1* expression on Affymetrix HgU95A microarrays. Compiled transcriptional profiling data from patients with infiltrating ductal carcinoma or benign breast disease were plotted. Gray columns, 50% range of the data surrounding the median; white lines within each column, median; black lines, outliers. Numbers under each column represent the number of samples analyzed. N, normal tissue; FC, fibrocystic breast disease; FA, fibroadenoma; and IDC, infiltrating ductal carcinoma. *B,* real-time reverse transcription-PCR analysis of matched sample pairs from patients with infiltrating ductal carcinoma. Gray columns, stage II carcinomas; open columns, stage III carcinomas; and black columns, adjacent normal tissue. T, tumor tissue; N, adjacent normal tissue. *C,* Western blot analysis of FoxM1 expression in breast epithelial cell lines. β-Actin is shown as a loading control.

We then measured proliferation in BT-20 and MCF-7 breast cancer cells with reduced FoxM1 expression. Cells were plated 24 hours after transfection and analyzed using WST-1, which measures mitochondrial dehydrogenase activity and reflects cell number. Both cell lines displayed a decrease in proliferation over the time course examined (Fig. 2*C* and *D*). BT-20 cells showed a maximal growth inhibition of 46% at 72 hours posttransfection, whereas the proliferation of MCF-7 cells was inhibited 39% at the same time point. Because the extent of growth inhibition was similar, it is likely that the level of FoxM1 protein in both cell lines was limiting for proliferation, even though the absolute level of expression differed. Another siRNA targeting FoxM1 showed similar growth inhibition in both cell lines (data not shown). We also attempted to determine whether FoxM1 is essential for proliferation in nontransformed epithelial cells. Our results indicate that transfection of MCF-12A cells with FoxM1 siRNA

does not decrease proliferation (data not shown). However, we were unable to detect a reduction in FoxM1 protein expression beyond the already low level in MCF-12A cells. Therefore, we cannot definitively establish the effect of lowering FoxM1 expression in nonmalignant cells.

RNAi of FoxM1 did not induce apoptosis in either breast cancer cell line, as determined by ELISA analysis of ssDNA at each time point analyzed in the proliferation assay (data not shown). Due to the lack of an increase in cell death, we hypothesized that decreased FoxM1 may have an effect on the cell cycle. Analysis of BT-20 cells at 48 hours posttransfection indicated an increase in the percentage of cells in G_2-M and a concomitant decrease in the G_1 population (Fig. 2*E*). No increase in the sub-G_1 population of cells was observed, confirming that there is no significant increase in apoptosis when cells are treated with FoxM1 siRNA. Analysis of cell cycle profiles at 72 and 120 hours posttransfection revealed identical profiles among mock, GFP, and FoxM1 transfected cells (data not shown). Therefore, FoxM1 siRNA induces a transient block in G_2, which is sufficient to alter the proliferation of BT-20 and MCF-7 cells.

FoxM1 regulates genes involved in transcription and cell cycle regulation. Although the role of FoxM1 in coupling S phase and mitosis has been observed, the transcriptional program by which FoxM1 regulates this function is not entirely clear. Previous studies have identified several cell cycle regulatory genes that are directly regulated by FoxM1 in reporter assays, including *cdc25B* (6), *cyclin B1* (2), and *cyclin D1* (26). In addition, mice expressing a liver-specific FoxM1 transgene show accelerated induction of cyclins B1, B2, A2, and F following partial hepatectomy (27). However, a genome-wide analysis of genes that are transcriptionally regulated by FoxM1 has not been reported. In order to identify additional genes that are regulated by FoxM1, we isolated RNA from BT-20 cells that had been transfected with FoxM1 siRNA and monitored expression of ~22,000 transcripts on Affymetrix HgU133A microarrays. Triplicate transfections were done for mock, GFP siRNA, and FoxM1 siRNA samples, and RNA was collected 48 hours after transfection. Approximately 50% (11,233) of the tiled transcripts were detectable in three or more samples, and these transcripts were used for further analysis as described in Materials and Methods. Using mock- and GFP-transfected cells as a control, we identified a set of 27 genes that was specifically regulated in cells transfected with FoxM1 siRNA (Table 1). The results indicate that *FoxM1* was the most differentially expressed gene, with a 5.69-fold decrease. Expression of other forkhead family members did not change significantly (Supplemental Fig. S2*A*), indicating that the FoxM1 siRNA specifically decreases expression of FoxM1. Included in the list were *cdc25B* and *cyclin A* (denoted CCNA2 in Fig. 3), two previously reported FoxM1 target genes. In addition, FoxM1 siRNA modulated several genes that are themselves involved in transcriptional regulation, including the WT-1 interacting protein *CIAO1*, the retinoblastoma-interacting protein *RBBP1*, and the transcriptional corepressor *DR1*. Also among the identified genes were two that are required for mitotic spindle assembly. *CENP-A* is a conserved variant of histone H3 and is implicated in kinetochore assembly (28). *Nek2* is a centrosomal kinase that is required for chromosome segregation and cytokinesis (29). Four

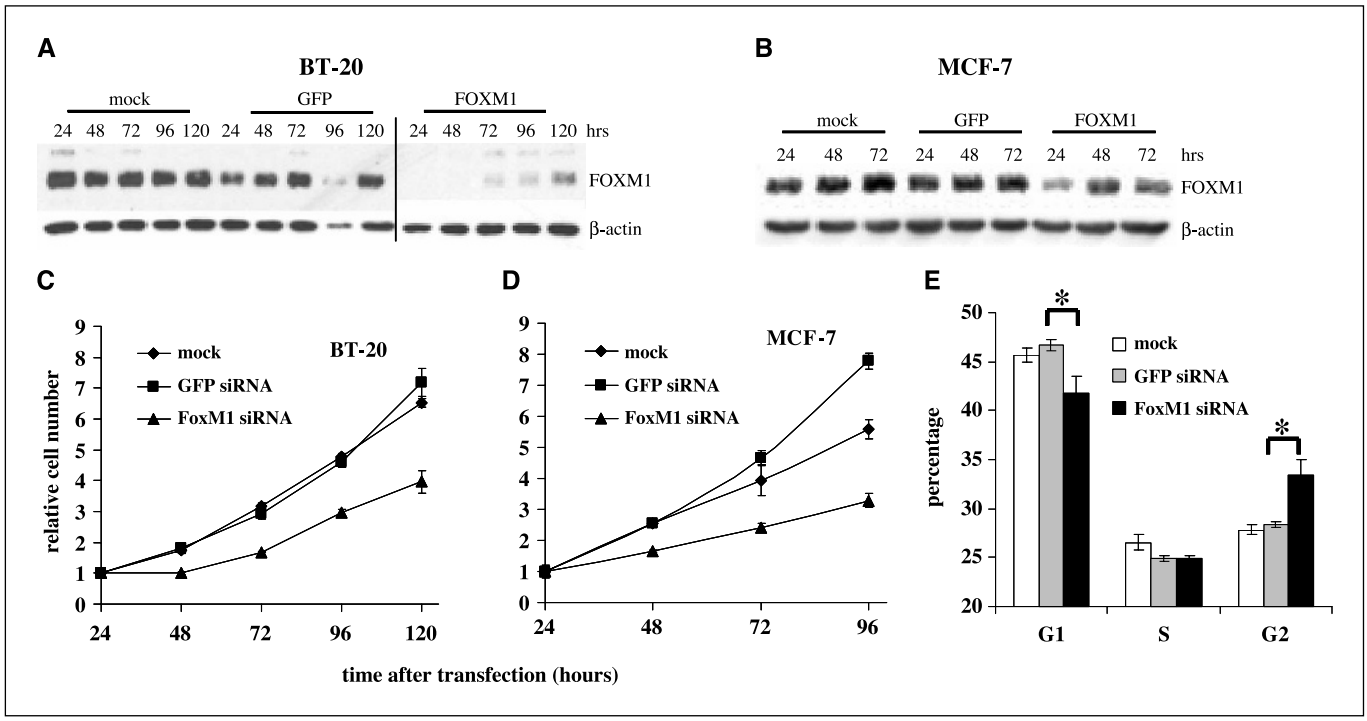

Figure 2. FoxM1 siRNA inhibits proliferation in BT-20 and MCF-7 breast cancer cell lines. *A* and *B,* depletion of FoxM1 protein by RNAi in breast cancer epithelial cells. Cells were transfected with lipid reagent only (mock), GFP, or FoxM1 siRNAs and cell lysates were collected at the indicated times. Immunoblot analysis was done with antibodies to FoxM1 or β-actin. BT-20 lysates (*A*) were loaded on two separate gels that were completed simultaneously (denoted by vertical black line). *C* and *D,* proliferation assay of cells transfected with FoxM1 siRNA. Cells were transfected with siRNA at $t = 0$ plated in 96-well plates 24 hours after transfection. WST-1 was used to measure cell number. Cell number is expressed as the ratio relative to the cell number at plating ($t = 24$ hours). *E,* cell cycle analysis of BT-20 cells 48 hours after transfection with lipid alone (mock), or siRNA targeting GFP or FoxM1. Triplicate samples were collected by trypsinization, stained with propidium iodide, and analyzed by flow cytometry. The percentage of cells in each phase of the cell cycle was determined with ModFit LT (Verity Software, Topsham, ME). *Columns*, mean; *bars*, SD. *, Student's *t* test, *P* value < 0.03.

genes were selected for analysis using real-time reverse transcription-PCR, and all four confirmed the microarray data (Supplemental Fig. S2*B*). These results suggest that in addition to cell-cycle regulatory genes, FoxM1 also regulates genes that are required for transcriptional control and mitosis.

Stable FoxM1 short hairpin RNA decreases cell viability. In order to evaluate the consequences of prolonged depletion of FoxM1, we transfected BT-20 cells with a stable construct expressing FoxM1 shRNA and evaluated cell viability with crystal violet staining, as diagramed in Fig. 3*A*. Figure 3*B* shows that the construct was effective in reducing both FoxM1 RNA and protein expression after 6 days in selection media. However, we were unable to isolate a stable cell line with reduced FoxM1 expression. Figure 3*C* shows that although cells were plated at the same density prior to selection (day 2), following selection for 6 days, there were fewer cells surviving after transfection with FoxM1 shRNA as compared with cells transfected with control shRNA (day 8). After 7 days of growth, control cells continued to proliferate, whereas the number of FoxM1 shRNA cells continued to decrease (day 15). The results indicate that disruption of FoxM1 affects cell survival and inhibits cellular proliferation.

Mitotic catastrophe and polyploidy are induced in FoxM1 short hairpin RNA cells. We hypothesized that defects in mitotic progression may be responsible for the extensive cell death following transfection with FoxM1 shRNA (Fig. 3*C*, days 8 and 15). Therefore, time-lapse microscopy was used to follow cells through mitosis. Figure 4*A* shows that a control cell initiates mitosis, undergoes cytokinesis, and returns to interphase within 120 minutes. In contrast, we found that there are two distinct outcomes for cells expressing FoxM1 shRNA. The majority of cells initiates mitosis but are unable to divide, eventually undergoing cell death while in mitosis (Fig. 4*B*). The morphology of these cells is identical to previously reported instances of mitotic catastrophe, including catastrophe induced by siRNA to hNuf2 (22) or ionizing radiation (30). In addition, 4′,6-diamidino-2-phenylindole staining of nuclei revealed multinucleation that is typical of mitotic catastrophe (Supplemental Fig. S3*A*). Therefore, we conclude that most of the cells with decreased FoxM1 expression enter mitosis but are unable to divide, and cell death results from mitotic catastrophe. A smaller population of cells initiates mitosis, does not divide, and exits mitosis without completing nuclear division or cytokinesis (Fig. 4*C*). These cells undergo a prolonged arrest after initiating mitosis, averaging 450 $\pm$ 150 minutes. This leads to the formation of enlarged cells with polyploid nuclei (Fig. 4*H*, 4′,6-diamidino-2-phenylindole-stained cells and Supplemental Fig. S3*B*), similar to the phenotype observed in hepatocytes and cardiomyoctes of *FoxM1* knock-out mice (3). Although this population of cells is able to complete several rounds of DNA replication in the absence of cell

Table 1. Microarray analysis of BT-20 cells transfected with FoxM1 siRNA

Probe set	Gene symbol	G_0 molecular function	Fold change	Fold change (*P*)
Transcription				
202580_x_at	*FOXM1*	RNA polymerase II transcription factor	−5.69	4.11E−06
209187_at	*DR1*	DNA binding, transcriptional corepressor	−3.92	1.41E−04
218490_s_at	*ZNF302*	DNA binding	−2.08	3.06E−03
203536_s_at	*CIAO1*	transcriptional regulation	−1.85	1.69E−03
209786_at	*HMGN4*	DNA binding	−1.80	2.01E−03
204080_at	*TOE1*	transcriptional repressor activity	−1.71	4.68E−05
205062_x_at	*RBBP1*	chromatin binding, transcription factor	1.70	5.28E−03
Cell cycle and chromosome segregation				
209714_s_at	*CDKN3*	protein phosphatase	−2.10	1.66E−06
201853_s_at	*CDC25B*	protein tyrosine phosphatase	−1.96	1.64E−04
218755_at	*KIF20A*	ATP binding, motor, protein transporter	−1.78	6.22E−04
211080_s_at	*NEK2*	kinase, cytokinesis, centrosome	−1.78	1.10E−03
203418_at	*CCNA2*	cyclin-dependent protein kinase	−1.77	4.67E−04
210821_x_at	*CENPA*	chromatin binding	−1.72	1.02E−03
Metabolism				
202382_s_at	*GNPI*	glucosamine-6-phosphate deaminase	−1.93	6.35E−03
205749_at	*CYP1A1*	cytochrome P450, oxidoreductase	−1.77	4.72E−03
217989_at	*RETSDR2*	oxidoreductase	−1.71	4.95E−04
Cytokine				
205767_at	*EREG*	epidermal growth factor receptor ligand	1.73	3.09E−04
202859_x_at	*IL8*	chemokine, interleukin-8 receptor ligand	1.84	9.33E−03
Other				
209885_at	*ARHD*	GTP binding, GTPase	−2.64	5.69E−04
219770_at	*FLJ11753*	glycosyltransferase-like	−2.58	2.25E−06
204944_at	*PTPRG*	tyrosine phosphatase	−2.06	1.45E−03
203414_at	*MMD*	macrophage maturation-associated	−1.88	2.00E−03
203890_s_at	*DAPK3*	kinase, induction of apoptosis	−1.76	2.50E−05
200699_at	*RPL23*	structural constituent of ribosome	−1.75	1.20E−03
212702_s_at	*BICD2*	microtubule dynamics	−1.74	6.06E−04
213478_at	*KIAA1026*	unknown	−1.73	8.85E−03
202627_s_at	*SERPINE1*	plasminogen activator, serpin	−1.72	7.55E−04

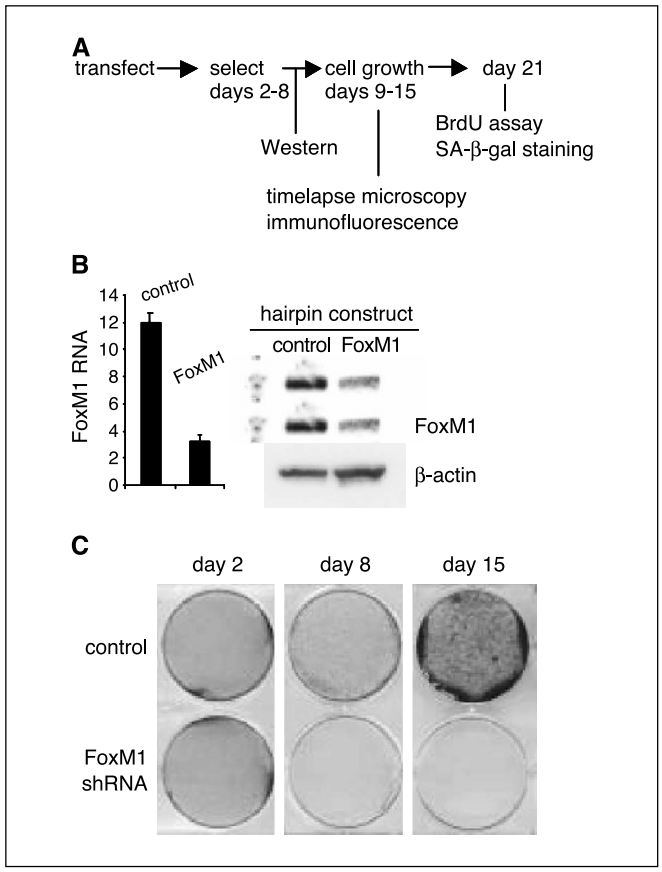

Figure 3. shRNA directed against FoxM1 decreases cell survival. *A,* experimental timeline for Figs. 4–6. *B,* real-time reverse transcription-PCR and Western blot analysis of FoxM1 expression after transfection with negative control shRNA or FoxM1 shRNA. Cells were collected at day 8 posttransfection. *C,* crystal violet staining of transfectants during (days 2 and 8) and after (day 15) selection with puromycin.

division, over time (21 days after transfection), these cells eventually undergo cell death, although the cells do not resemble traditional apoptotic or necrotic cells (Fig. 4*E-G*). Instead, the cells display the enlarged, flattened morphology associated with cellular senescence. Therefore, cells were stained for the presence of SA-β-gal activity, a well-characterized marker of senescence (31). Neither control nor FoxM1 shRNA cells were positive in this assay (data not shown). We also analyzed BrdU incorporation to determine whether the cells are actively proliferating. At 21 days posttransfection, negative control cells were 85% positive for BrdU, whereas the percentage of positive cells dropped to 40% when FoxM1 expression was reduced (Fig. 4*H*). We conclude that although a minor population of FoxM1 shRNA cells is able to undergo endoreduplication, these cells eventually lose their capacity to replicate DNA and undergo cell death.

Depletion of FoxM1 induces mitotic spindle aberrations. In order to establish whether defective spindle formation plays a role in the mitotic failure of cells transfected with FoxM1 shRNA, the mitotic spindle was examined using α-tubulin antibodies to stain microtubules. Figure 5*A* indicates a control cell in mitosis, with a typical bipolar spindle. Figure 5*B-D* represent various mitotic abnormalities found in FoxM1 shRNA-transfected cells. Figure 5*B* is a representative example of a metaphase cell that contains condensed chromatin but lacks an organized mitotic spindle, with multiple apparent spindle poles throughout the cell. Figure 5*C* and *D* indicate an organized tripolar or tetrapolar spindle, respectively, that is typically seen in cells with reduced FoxM1 expression. Quantitative analysis of mitotic cells stained with α-tubulin antibodies indicates that 21.0 ± 3.6% of control cells versus 62.6 ± 4.5% of FoxM1 shRNA cells exhibit mitotic spindle defects.

Because centrosomes play a critical role in bipolar spindle organization, we investigated whether the defects in spindle formation were due to centrosomal amplification using antibodies to γ-tubulin, a core component of the centrosome (32). Figure 6*A* shows that control cells contain two centrosomes during interphase, and form a bipolar mitotic spindle. Figure 6*B* indicates that FoxM1 shRNA cells contain numerous centrosomes during interphase, which leads to the formation of multiple spindle poles in mitotic cells (Fig. 6*C-E*). The results indicate that some centrosomes are able to nucleate microtubules whereas others remain unattached to the mitotic spindle (Fig. 6*C* and *D*, white arrows). This explains our observation that although most cells displaying centrosome amplification contain 10 or more visible centrosomes during interphase, the formation of mitotic spindles with more than five poles was not observed. Evaluation of at least 200 cells from triplicate transfections determined that the percentage of cells with more than two centrosomes was 19.2 ± 1.3% in control cells versus 63.0 ± 4.0% in FoxM1 shRNA cells. Therefore, depletion of FoxM1 significantly increases centrosome number. Our results suggest that FoxM1 shRNA cells undergo mitotic catastrophe due to the formation of multipolar spindles that nucleate from supernumerary centrosomes.

Discussion

Elevated expression of *FoxM1* has previously been found in hepatocellular carcinoma (9) and basal cell carcinoma (8). Further evidence linking FoxM1 with malignant transformation is provided by the recent finding that mice with a conditional deletion of *FoxM1* in hepatocytes are resistant to developing hepatocellular carcinomas following exposure to a diethylnitrosamine/phenobarbital tumor induction protocol (10). We report here that microarray analysis of 194 infiltrating ductal carcinomas indicates that *FoxM1* expression is also increased in breast cancer, and the increase is significant relative to both normal tissue and benign breast disease. TaqMan RT-PCR analysis of matched pairs of tumor and adjacent normal tissue confirms the microarray data and indicates that *FoxM1* expression is higher in stage III than in stage II carcinomas. However, whether *FoxM1* expression is clinically useful for staging remains to be determined.

Using RNA interference, we have shown that reducing FoxM1 expression is sufficient to inhibit the proliferation of breast cancer cell lines and cause an increase in the population of cells in G_2-M. Previous studies using a tetracycline-inducible HeLa cell line indicated that FoxM1 overexpression does not affect the cell cycle under normal serum conditions in unsynchronized cells (2). However, following serum deprivation, FoxM1 expression facilitated growth recovery and also accelerated the exit from G_2-M following synchronization with L-mimosine. Our results indicate that FoxM1 expression is necessary for the proliferation of breast cancer epithelial cells under normal serum conditions in logarithmically growing cells. Prolonged depletion of FoxM1 inhibits proliferation and also decreases cell viability, suggesting that this is an effective mechanism for eliminating transformed cells.

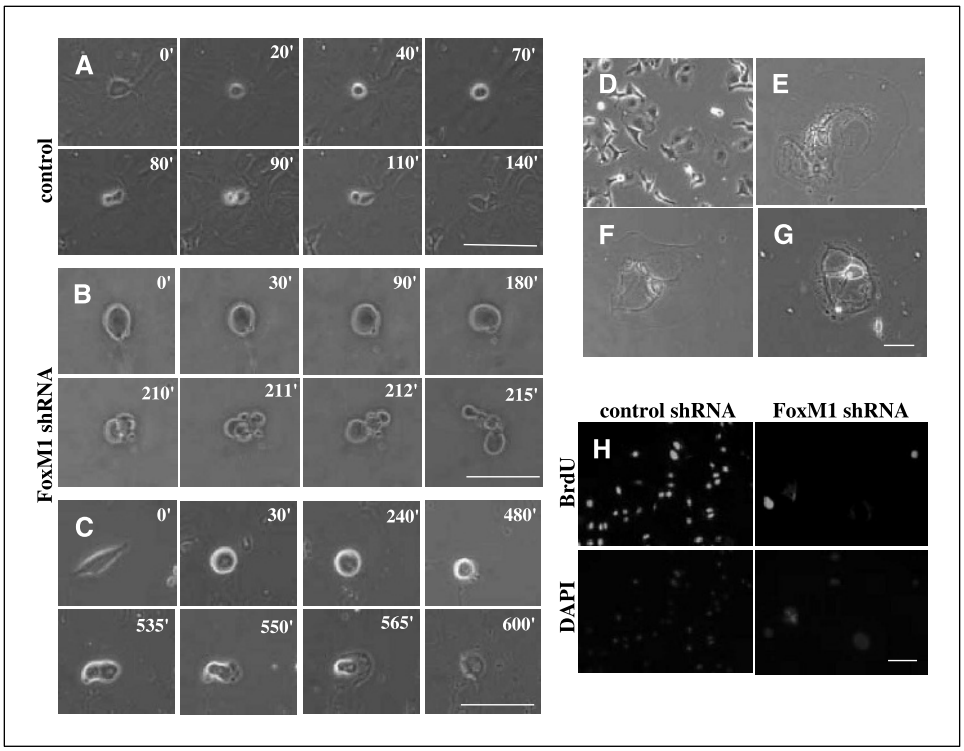

Figure 4. FoxM1 shRNA inhibits cell cycle progression and induces mitotic catastrophe. *A,* time-lapse microscopy of mitotic BT-20 cells stably transfected with control shRNA (*A*) or FoxM1 shRNA (*B* and *C*). Images were collected at regular intervals over the course of the experiment, and selected images are shown. *D-G,* phase contrast images of BT-20 cells at 3 weeks posttransfection. All images are at the same magnification. *D,* BT-20 cells stably transfected with control shRNA. *E-G,* BT-20 cells stably transfected with FoxM1 shRNA. Cells at this stage were negative for SA-β-gal activity. *H,* analysis of BrdUrd incorporation. Cells were labeled with BrdUrd for 20 hours and stained with anti-BrdUrd antibody (*green*) and counterstained with 4′,6-diamidino-2-phenylindole (*blue*). All images are at the same magnification. *Bars*, 100 μm.

We hypothesized that identification of genes regulated by FoxM1 would facilitate an understanding of the role FoxM1 plays in cell cycle progression. The microarray results provide insight into how FoxM1 may affect both the G_1-S and G_2-M transition. One of the genes we identified, *RBBP1*, inhibits the G_1-S transition by binding to retinoblastoma and recruiting histone deacetylases, resulting in decreased expression of genes regulated by E2F (33). Therefore, repression of *RBBP1* by FoxM1 would promote progression into S phase. *CDKN3* and cyclin A2, which are regulated by FoxM1, also play a role in the progression from G_1 to S phase by binding to CDK2. Cyclin A binding to CDK2 promotes S phase progression (34), whereas expression of CDKN3, which binds and inactivates CDK2, inhibits entry into S phase (35). Although CDKN3 activity is associated with cell cycle arrest, its expression is elevated in both breast and prostate cancer. In addition, lowering CDKN3 expression reduces anchorage-independent growth and tumor formation in nude mice (36), suggesting that CDKN3 is associated with the transformed phenotype. FoxM1 also plays a role in regulating G_2-M by inducing expression of *cyclin A* and *cdc25B*. Cyclin A binding to CDK1 promotes entry into mitosis (34), whereas cdc25B dephosphorylates CDK1, thereby promoting CDK1 activity.

Several of the identified genes provide a molecular pathway linking FoxM1 to mitotic progression and spindle formation. CENP-A is essential for centromere structure and function, as indicated by the observation that RNAi of CENP-A causes a failure of chromosome alignment at the metaphase plate (37). In addition, CENP-A is overexpressed in colorectal cancer (38). Expression of KIF20A, a microtubule-associated motor protein, is up-regulated in mitosis and localizes to the spindle midzone during anaphase (39). Cells injected with antibodies against KIF20A become binucleate, indicating that KIF20A is required for cytokinesis. Another gene identified on the microarray, *NEK2*, localizes to centrosomes throughout the cell cycle and overexpression triggers centrosome splitting in U2OS cells (40). It is also notable that two of the genes regulated by FoxM1, *cyclin A* and *cdc25B*, have been implicated in centrosome regulation. The cyclin A/CDK2 complex is required for centrosome duplication (41), and Aurora A phosphorylates cdc25B in mitotic cells, localizing cdc25B to the centrosome (42). Although

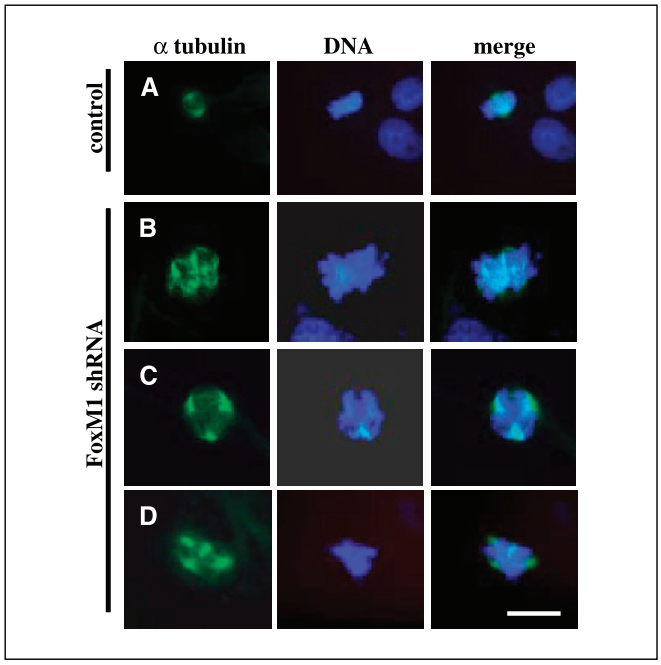

Figure 5. Mitotic spindle abnormalities in FoxM1 shRNA BT-20 cells. *A,* typical appearance of control shRNA cells. *B-D,* cells transfected with FoxM1 shRNA. The first column shows staining for microtubules with α-tubulin antibodies, the second column shows DNA stained with 4′,6-diamidino-2-phenylindole, and the third column is a merged image. *Bar*, 20 μm.

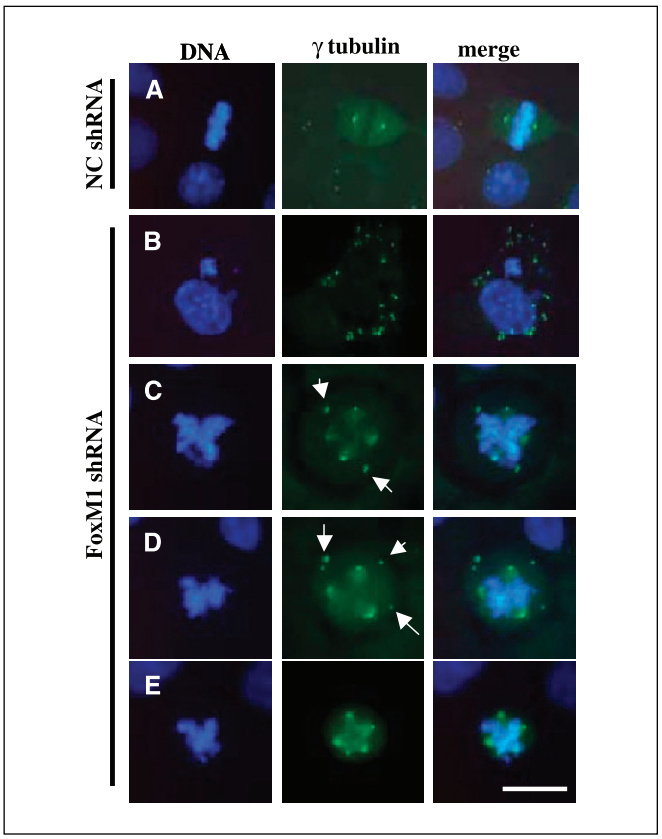

Figure 6. FoxM1 shRNA induces centrosomal amplification. Cells were fixed and stained with monoclonal antibody to γ-tubulin, an integral component of the centrosome. The first column shows centrosomes, the second column is DNA stained with 4′,6-diamidino-2-phenylindole, and the third column is a merged image. White arrows, centrosomes that are not functioning as microtubule organizing centers. *Bar*, 20 μm.

most of these putative FoxM1 target genes contain at least one of the potential FoxM1 binding sites reported in the literature (4, 5, 25), it is possible that some of the genes we identified are not direct targets of FoxM1 but are deregulated as a result of aberrant cell cycle progression. This issue necessitates further study to determine whether FoxM1 directly regulates these genes.

Several recent studies have indicated that polyploidy is often associated with centrosomal amplification. Inactivation of E2F3 (43) or overexpression of Aurora A (44) leads to centrosomal amplification accompanied by polyploidy. A further example is provided by MEF cells with a targeted deletion of the ubiquitin ligase component *Skp2*, which display polyploidy, centrosomal amplification, and increased apoptosis (45). Our results also indicate that centrosomal amplification occurs concomitantly with polyploidy, because we did not observe elevated centrosome numbers unless cells also contained enlarged, polyploid nuclei. Because we observed defects in mitotic progression and cytokinesis, the centrosome abnormalities seem to be a result of polyploidy, rather than implicating FoxM1 directly in the control of centrosome duplication. Nevertheless, the generation of multiple spindle poles seems to be incompatible with cell viability and leads to cell death by mitotic catastrophe.

The data presented here indicate that inhibition of FoxM1 represents an attractive target for cancer therapy. Because overexpression has been noted in hepatocellular carcinoma, basal cell carcinoma, and infiltrating ductal carcinoma, a FoxM1 inhibitor has the potential for efficacy in several types of tumors. In addition, low FoxM1 expression in normal adult tissues, coupled with the observation that *FoxM1*$^{-/-}$ mice are normal with the exception of hepatocytes and cardiomyoctes, indicates that therapeutic intervention should have minimal toxicity in normal cells. Rather than inducing cell cycle arrest, continuous loss of FoxM1 is cytotoxic and has the potential to completely eliminate tumor cells. Our results indicate that inhibiting FoxM1 presents a mechanism to selectively target transformed cells that are dependent on FoxM1 for survival.

Acknowledgments

Received 11/11/2004; revised 3/6/2005; accepted 3/18/2005.

The costs of publication of this article were defrayed in part by the payment of page charges. This article must therefore be hereby marked *advertisement* in accordance with 18 U.S.C. Section 1734 solely to indicate this fact.

We thank Yizheng Li for statistical expertise, Veronica Diesl for assistance with the human tumor samples, and Chi Dang, Andy Dorner, and Tim Haggerty for helpful comments on the manuscript.

References

1. Westendorf JM, Rao PN, Gerace L. Cloning of cDNAs for M-phase phosphoproteins recognized by the MPM2 monoclonal antibody and determination of the phosphorylated epitope. Proc Natl Acad Sci U S A 1994;91:714–8.
2. Leung TW, Lin SS, Tsang AC, et al. Over-expression of FoxM1 stimulates cyclin B1 expression. FEBS Lett 2001;507:59–66.
3. Korver W, Schilham MW, Moerer P, et al. Uncoupling of S phase and mitosis in cardiomyocytes and hepatocytes lacking the winged-helix transcription factor Trident. Curr Biol 1998;8:1327–30.
4. Korver W, Roose J, Clevers H. The winged-helix transcription factor Trident is expressed in cycling cells. Nucleic Acids Res 1997;25:1715–9.
5. Yao KM, Sha M, Lu Z, Wong GG. Molecular analysis of a novel winged helix protein, WIN. Expression pattern, DNA binding property, and alternative splicing within the DNA binding domain. J Biol Chem 1997;272:19827–36.
6. Wang X, Kiyokawa H, Dennewitz MB, Costa RH. The Forkhead Box m1b transcription factor is essential for hepatocyte DNA replication and mitosis during mouse liver regeneration. Proc Natl Acad Sci U S A 2002;99:16881–6.
7. Ye H, Holterman AX, Yoo KW, Franks RR, Costa RH. Premature expression of the winged helix transcription factor HFH-11B in regenerating mouse liver accelerates hepatocyte entry into S phase. Mol Cell Biol 1999;19:8570–80.
8. Teh MT, Wong ST, Neill GW, Ghali LR, Philpott MP, Quinn AG. FOXM1 is a downstream target of Gli1 in basal cell carcinomas. Cancer Res 2002;62:4773–80.
9. Okabe H, Satoh S, Kato T, et al. Genome-wide analysis of gene expression in human hepatocellular carcinomas using cDNA microarray: identification of genes involved in viral carcinogenesis and tumor progression. Cancer Res 2001;61:2129–37.
10. Kalinichenko VV, Major ML, Wang X, et al. Foxm1b transcription factor is essential for development of hepatocellular carcinomas and is negatively regulated by the p19ARF tumor suppressor. Genes Dev 2004;18:830–50.
11. Hinchcliffe EH, Sluder G. "It takes two to tango": understanding how centrosome duplication is regulated throughout the cell cycle. Genes Dev 2001;15:1167–81.
12. Hinchcliffe EH, Miller FJ, Cham M, Khodjakov A, Sluder G. Requirement of a centrosomal activity for cell cycle progression through G_1 into S phase. Science 2001;291:1547–50.
13. Khodjakov A, Rieder CL. Centrosomes enhance the fidelity of cytokinesis in vertebrates and are required for cell cycle progression. J Cell Biol 2001;153:237–42.
14. Lingle WL, Barrett SL, Negron VC, et al. Centrosome amplification drives chromosomal instability in breast tumor development. Proc Natl Acad Sci U S A 2002;99:1978–83.
15. Pihan GA, Purohit A, Wallace J, et al. Centrosome defects and genetic instability in malignant tumors. Cancer Res 1998;58:3974–85.
16. Liang YX, Zhang W, Li DD, et al. Mitotic cell death in BEL-7402 cells induced by enediyne antibiotic lidamycin is associated with centrosome overduplication. World J Gastroenterol 2004;10:2632–6.
17. Castedo M, Perfettini JL, Roumier T, Andreau K, Medema R, Kroemer G. Cell death by mitotic catastrophe: a molecular definition. Oncogene 2004;23:2825–37.
18. Zhou BB, Elledge SJ. The DNA damage response: putting checkpoints in perspective. Nature 2000;408:433–9.

19. Chan TA, Hermeking H, Lengauer C, Kinzler KW, Vogelstein B. 14-3-3σ is required to prevent mitotic catastrophe after DNA damage. Nature 1999;401:616–20.

20. Brown EJ, Baltimore D. ATR disruption leads to chromosomal fragmentation and early embryonic lethality. Genes Dev 2000;14:397–402.

21. Takai H, Tominaga K, Motoyama N, et al. Aberrant cell cycle checkpoint function and early embryonic death in Chk1(−/−) mice. Genes Dev 2000;14:1439–47.

22. DeLuca JG, Moree B, Hickey JM, Kilmartin JV, Salmon ED. hNuf2 inhibition blocks stable kinetochore-microtubule attachment and induces mitotic cell death in HeLa cells. J Cell Biol 2002;159:549–55.

23. Lockhart DJ, Dong H, Byrne MC, et al. Expression monitoring by hybridization to high-density oligonucleotide arrays. Nat Biotechnol 1996;14:1675–80.

24. Hill AA, Brown EL, Whitley MZ, Tucker-Kellogg G, Hunter CP, Slonim DK. Evaluation of normalization procedures for oligonucleotide array data based on spiked cRNA controls RESEARCH0055. Genome Biol 2001;2.

25. Ye H, Kelly TF, Samadani U, et al. Hepatocyte nuclear factor 3/fork head homolog 11 is expressed in proliferating epithelial and mesenchymal cells of embryonic and adult tissues. Mol Cell Biol 1997;17:1626–41.

26. Wang X, Quail E, Hung NJ, Tan Y, Ye H, Costa RH. Increased levels of forkhead box M1B transcription factor in transgenic mouse hepatocytes prevent age-related proliferation defects in regenerating liver. Proc Natl Acad Sci U S A 2001;98:11468–73.

27. Wang X, Hung NJ, Costa RH. Earlier expression of the transcription factor HFH-11B diminishes induction of p21(CIP1/WAF1) levels and accelerates mouse hepatocyte entry into S-phase following carbon tetrachloride liver injury. Hepatology 2001;33:1404–14.

28. Howman EV, Fowler KJ, Newson AJ, et al. Early disruption of centromeric chromatin organization in centromere protein A (Cenpa) null mice. Proc Natl Acad Sci U S A 2000;97:1148–53.

29. Faragher AJ, Fry AM. Nek2A kinase stimulates centrosome disjunction and is required for formation of bipolar mitotic spindles. Mol Biol Cell 2003;14:2876–89.

30. Nitta M, Kobayashi O, Honda S, et al. Spindle checkpoint function is required for mitotic catastrophe induced by DNA-damaging agents. Oncogene 2004.

31. Dimri GP, Lee X, Basile G, et al. A biomarker that identifies senescent human cells in culture and in aging skin *in vivo*. Proc Natl Acad Sci U S A 1995;92:9363–7.

32. Wiese C, Zheng Y. γ-Tubulin complexes and their interaction with microtubule-organizing centers. Curr Opin Struct Biol 1999;9:250–9.

33. Lai A, Marcellus RC, Corbeil HB, Branton PE. RBP1 induces growth arrest by repression of E2F-dependent transcription. Oncogene 1999;18:2091–100.

34. Strausfeld UP, Howell M, Descombes P, et al. Both cyclin A and cyclin E have S-phase promoting (SPF) activity in *Xenopus* egg extracts. J Cell Sci 1996;109:1555–63.

35. Gyuris J, Golemis E, Chertkov H, Brent R. Cdi1, a human G_1 and S phase protein phosphatase that associates with Cdk2. Cell 1993;75:791–803.

36. Lee SW, Reimer CL, Fang L, Iruela-Arispe ML, Aaronson SA. Overexpression of kinase-associated phosphatase (KAP) in breast and prostate cancer and inhibition of the transformed phenotype by antisense KAP expression. Mol Cell Biol 2000;20:1723–32.

37. Goshima G, Kiyomitsu T, Yoda K, Yanagida M. Human centromere chromatin protein hMis12, essential for equal segregation, is independent of CENP-A loading pathway. J Cell Biol 2003;160:25–39.

38. Tomonaga T, Matsushita K, Yamaguchi S, et al. Overexpression and mistargeting of centromere protein-A in human primary colorectal cancer. Cancer Res 2003;63:3511–6.

39. Fontijn RD, Goud B, Echard A, et al. The human kinesin-like protein RB6K is under tight cell cycle control and is essential for cytokinesis. Mol Cell Biol 2001;21:2944–55.

40. Fry AM, Meraldi P, Nigg EA. A centrosomal function for the human Nek2 protein kinase, a member of the NIMA family of cell cycle regulators. EMBO J 1998;17:470–81.

41. Meraldi P, Lukas J, Fry AM, Bartek J, Nigg EA. Centrosome duplication in mammalian somatic cells requires E2F and Cdk2-cyclin A. Nat Cell Biol 1999;1:88–93.

42. Dutertre S, Cazales M, Quaranta M, et al. Phosphorylation of CDC25B by Aurora-A at the centrosome contributes to the G_2-M transition. J Cell Sci 2004;117:2523–31.

43. Saavedra HI, Maiti B, Timmers C, et al. Inactivation of E2F3 results in centrosome amplification. Cancer Cell 2003;3:333–46.

44. Meraldi P, Honda R, Nigg EA. Aurora-A overexpression reveals tetraploidization as a major route to centrosome amplification in $p53^{-/-}$ cells. EMBO J 2002;21:483–92.

45. Nakayama K, Nagahama H, Minamishima YA, et al. Targeted disruption of Skp2 results in accumulation of cyclin E and p27(Kip1), polyploidy and centrosome overduplication. EMBO J 2000;19:2069–81.